Published in Engineering Fracture Mechanics, 2008, Vol. 75, p. 1605 - 1622, http://dx.doi.org/10.1016/j.engfracmech.2007.06.011

Prediction of fretting crack propagation based on a short crack methodology

S. Fouvry [a], D. Nowell [b], K.J. Kubiak [a], D.A. Hills [b]

[a] : LTDS, Ecole Centrale de Lyon, Ecully 69134 Cedex, France

[b] : Department of Engineering Science, University of Oxford, Parks Road,

krzysztof@kubiak.co.uk

Abstract :

Fretting tests have been conducted to determine the maximum crack extension under partial slip conditions, as a function of the applied tangential force amplitude. An analytical model representing a fretting-induced slant crack has been implemented and combined with the Kitagawa-Takahashi short crack methodology. This approach provides reasonable qualitative agreement between experimental and predicted maximum fretting crack lengths, supporting previous results concerning the prediction of the fretting–fatigue endurance. It is, however, observed that the model is systematically conservative. A discussion of the appropriate fundamental parameters when dealing with steep stress gradients such as those present in fretting, and which are difficult to interpret in the context of the Kitagawa-Takahashi method, is presented. It is shown that an inverse procedure identifies the required fundamental parameters. Hence, a specific fretting long crack transition length for the low carbon steel studied can be extrapolated. It is also shown that the maximum crack length evolution under plain fretting wear test conditions can be used to calibrate fretting fatigue predictions.

Keywords : Crack arrest, Fretting cracking, Kitagawa-Takahashi diagram, short cracks, AISI 1034 steel.

1. Introduction

Fretting is a small amplitude oscillatory movement, which may occur between contacting surfaces subjected to vibration or cyclic stress. Fretting is therefore encountered in assemblies of components subjected to vibration, and thus concerns a wide range of industries (e.g. helicopters, aircraft, trains, ships, trucks and electrical connectors) [1]. Fretting

damage on the contacting surface is critically controlled, under sliding conditions, by the amplitude of slip displacement [2, 3]. Under large amplitude gross slip conditions, where the whole surface is fretted and wear processes associated with debris formation and ejection dominate, friction energy wear models have been introduced [4]. Under partial slip conditions, initiation of fatigue cracks is generally a more significant concern than wear. Fretting fatigue tests, which combine a fretting contact and bulk fatigue loading, are classically used to investigate this regime [5]. The fretting and bulk fatigue loading are inter-dependent, and this feature complicates the investigation of their respective impacts. Fretting fatigue has a strong influence on both crack nucleation and early propagation, whereas bulk loading controls subsequent 'long crack' propagation [5]. Hence a sequential strategy involving crack nucleation, short crack propagation and long crack propagation approaches has been developed [5, 6, 7].

Because of the very severe stress gradients imposed on the contact surface, a direct application of a fatigue analysis based on a stress *at a given point* is not appropriate. Therefore, approaches which take a length scale into account need to be considered, combining either a stress-averaging process volume [8, 9] or an equivalent notch similitude description [10]. Prediction of subsequent crack propagation, and conditions for potential crack arrest, is less well understood [7, 11]. Crack propagation is generally affected by the contact loading as well by the bulk remote load. If a linear elastic fracture mechanics approach is adopted, most of the literature suggests that the crack will arrest if the stress intensity range ΔK falls below a threshold value (ΔK_{th}) [12]. The critical question then becomes: 'What is the threshold value?'. It has been extensively reported that short cracks propagate at nominal stress intensity levels below the long crack threshold [13]. Araújo and Nowell [7] applied a method based on the Kitagawa-Takahashi diagram [13] to resolve the paradox of propagating short fretting cracks. An alternative starting point, employing a 'short crack correction', was developed by El Haddad et al. [14] and may be used to predict fatigue thresholds. It may be shown that the two approaches are essentially similar: the former modifies the threshold, whereas the latter modifies the crack driving force. However, as noted in [7], a definitive validation of the concept will require a comparison of the experimental and predicted maximum crack extension beneath a contact. The purpose of the research reported here is therefore to investigate this aspect by combining well-defined fretting experiments with a detailed model of crack evolution, taking into account crack location and orientation.

To simplify the analysis, a single 2D cylinder/plane fretting geometry has been chosen, under purely alternating load. This allows a systematic crack arrest condition to be investigated, and simplifies the stress analysis. By comparing the experimental crack propagation with the evolution of the calculated mixed mode stress intensity factor, the stability of the short crack arrest methodology has been evaluated. The experiments were carried out using a well-defined low carbon steel has been studied in order to provide the material parameters required for the analysis.

2. Experimental procedure

2.1 Test system

The experimental setup used in this study is based on a fretting device rigidly mounted on to a servo hydraulic test machine (Fig.1). Further details of this setup and the experimental methods used can be found in [8, 15].

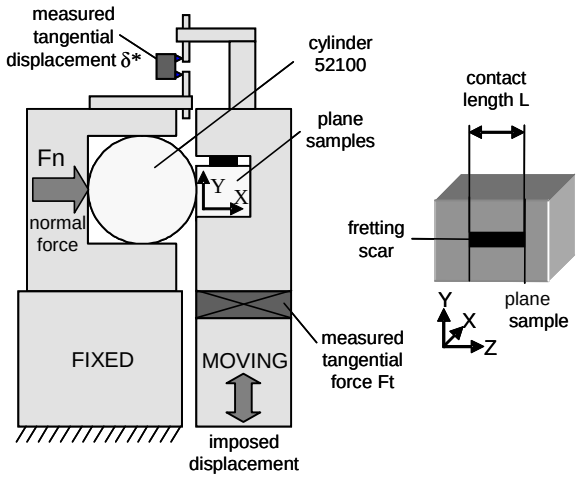

Fig.1. Schematic of the fretting test device and definition of the loading directions.

A partial-slip cylinder-on-flat contact configuration was used. Fretting was applied by imposing a nominally static normal force, F_n, followed by a purely alternating cyclic displacement amplitude ($\delta*$). As a consequence an alternating cyclic tangential load (F_t) was generated on the contact surface. During a test, F_n, F_t and δ were recorded, from which the δ - F_t fretting cycle can be plotted; this cycle is characterized respectively by the tangential force (F_t) and slip displacement (δ^*) amplitude. The radius of the 521000 steel cylinder is R = 40

mm and the pad length L = 5 mm, giving plane strain conditions near the central axis of the fretting scar (Fig.1b). The normal load was kept constant in all tests at $P=F_n/L$= 540 N/mm, equivalent to a peak contact pressure, p_0, of 700 MPa and a contact half-width, a, of 500 µm. Fretting tests were performed under constant-amplitude displacement at a frequency of 40 Hz. Note that under stabilized (steady state) partial slip conditions, a quasi-linear relationship exists between the displacement and tangential force amplitude. By exploiting this behavior, the imposed displacement amplitude was adjusted to monitor constant tangential force amplitudes ($Q^* = F_t/L$).

2.2 Material

The material used for the plane specimen was a low carbon steel alloy AISI 1034 which, after a specified heat treatment, provides the mechanical and fatigue properties listed in Table 1. An extensive fatigue investigation of this alloy was previously performed by Gros et al, under various stress ratio conditions, to evaluate the closure effect on short crack propagation [16]. The fatigue limit, σ_{fl}, and conventional long crack threshold, ΔK_0, under a fully reversing load (R= -1) are used to represent the fretting condition. Chromium 52100 steel was chosen for the cylindrical counterbody in order to ensure elastically similar conditions whilst simultaneously ensuring that cracks arose only in the AISI 1034 specimen.

Table 1 : Mechanical properties of the materials

Materials	E (GPa)	ν	σ_Y (0.2%) (MPa)	σ_{UTS} (MPa)	σ_{fl} (MPa) (R=-1, 10^7 cycles)	ΔK_0 (R=-1) (MPa$\sqrt{m}$)
AISI 1034 [16] (plane)	200	0.3	350	600	270 ± 10	7 ± 1
52100 [8] (cylinder)	210	0.3	1700	2000		

2.3 Contact configuration and post-test investigation

Figure 2 shows the detailed contact geometry used. In order to minimise edge-effects, the contact pad thickness and the transverse width of the plane specimen were machined to the

same dimension. Hence, whilst the side faces of the contact are traction-free, approximately plane-strain conditions are present along the centerline of the contact. This means that the pressure distribution decreases from a maximum value along the central region to a lower value towards the contact ends and eliminates any stress singularity problems [17]. Finally, the surfaces in contact were carefully polished to a mirror state (R_a around 0.05 μm).

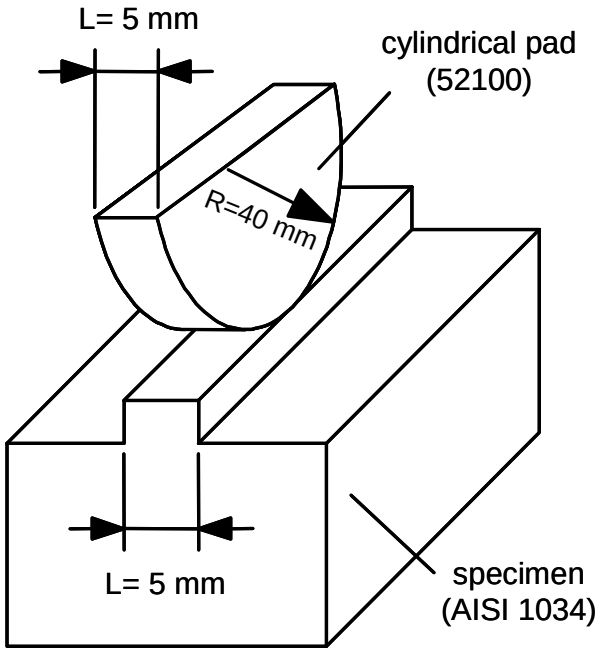

Fig. 2 : Detailed geometry of the contact.

After each fretting test, the following procedure was used to measure the crack depth and angle below the surface: the dimensions of the fretting scar were recorded and a section taken to reveal the x-y plane (Fig 1) running through the centre of the contact zone. The cut section was then polished and, from photographic images of the cross-section, the crack length and angle were measured.

A representative optical cross-section of fretting cracks is shown in Fig.3 and a single dominant fretting crack is clearly visible. The expertise of 8 cracked fretting scars obtained between 205 and 290 N/mm linear tangential force amplitudes concludes that the crack nucleates at the contact edge and propagates initially at an angle of about 30° ± 3 to the normal to the surface. The contact edge location has been confirmed by expertizing quasi undamaged contacts (i.e. incipient crack nucleation or short crack situations). It must be outlined the difficulty to relate the crack location for long crack situations. Indeed, the presence of a long crack through the interface significantly modifies the contact compliance

which promotes a significant increase of the contact area and complicates the analysis. Hence a crack initially nucleated at the contact borders can successively be observed through the inner part of the contact. In the present investigation the crack propagation range is limited and the contact edge localisation has been confirmed even for the longest crack situations.

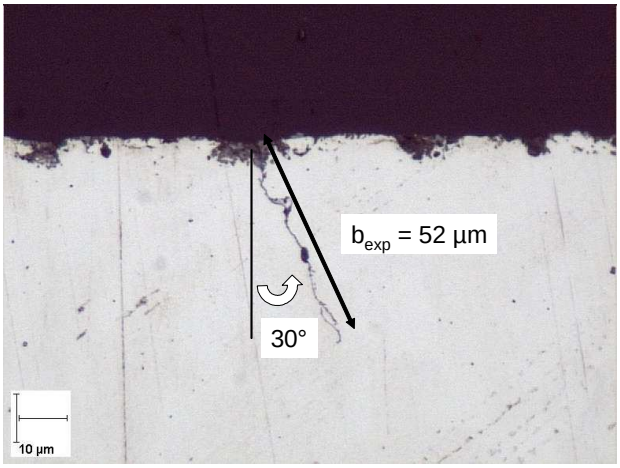

Fig. 3 : Optical of cross section along the central x-y plane of the fretting scar (P= 540 N/mm *, Q*=282* N/mm*, 10^6 cycles); b_{exp} : experimental maximum crack length.*

3. Friction and cracking analysis

3.1 Identification of the friction coefficient at the sliding transition

The stress analysis of the crack is critically affected by the value chosen for the friction coefficient. Hence, it is important to identify the evolution of this parameter value as a function of number of cycles as well as any spatial variation. Different approaches have been developed to achieve this [7, 18]. However, a recent study shows that the friction coefficient measured at the transition between partial and gross slip conditions (μ_t) may be used to provide representative value of the friction under partial slip condition (i.e. $\mu_{PS} \approx \mu_t$) [19]. To determine the sliding transition of the studied contact, a variable displacement method was used [19]: the normal load is kept constant whereas the relative displacement amplitude (δ^*) starts from a very low value, imposing a clear partial slip condition (with $Q^* < \mu.P$). When stabilized conditions are reached, δ^* is increased and then maintained constant until a new stable situation is reached. The imposed displacement, δ^*, is increased in this way, step by step, until the contact makes the transition to sliding ($Q^* = \mu.P$) (Fig. 4).

Published in Engineering Fracture Mechanics, 2008, Vol. 75, p. 1605 - 1622, http://dx.doi.org/10.1016/j.engfracmech.2007.06.011

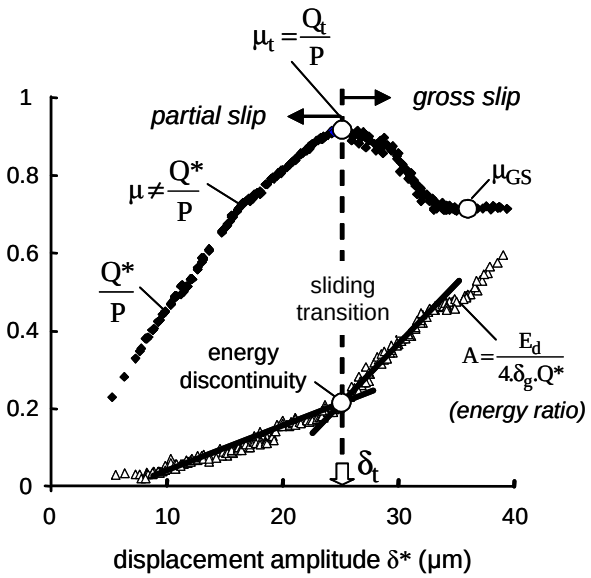

Fig. 4 : Illustration of variable displacement method applied to the contact conditions studied (see the text for detail). The ratio Q/P is increased until a stabilized gross slip condition is just reached. The energy ratio A is computed and exhibits a discontinuity at the transition.*

An accurate value for δ* at the transition is then calculated by computing the value of the energy sliding criterion $A = E_d/E_t$, where. E_d is the frictional energy dissipated during the critical cycle, and $E_t = 4.Ft.\delta^*$ the total energy, i.e. the external work done [18]). It has been shown that this ratio is a constant value for the sphere/plane configuration and related to a discontinuity in slope for the 2D cylinder/plane configuration (Fig. 4.) [19]. By identifying such a discontinuity the measured transition amplitude, δ_t, and the friction coefficient at the sliding transition can be identified. Several tests were performed which suggested $\mu_t = 0.9\pm 0.05$ may be taken as representative of the stabilized AISI 1034 / 52100 partial slip friction coefficient.

3.2 Identification of the number of fretting cycles associated with the crack arrest condition

In using the self-arrest model, we must be sure of the number of cycles needed to grow a crack to the point where the crack tip stress intensity falls below the threshold value. An initial series of nine tests was performed at a tangential force amplitude of Q* = 283 N/mm equivalent to 56% of the sliding transition tangential force.

Each test in the series was stopped at a different number of cycles, ranging between 2.5 x 10^5 and 3 x 10^6. Figure 5 shows the evolution of the maximum crack length with the number of fretting cycles for this series of tests. It may be seen that the crack length does not appear to increase after 10^6 fretting cycles, reaching a stabilized value. This value was therefore chosen as the critical number of cycles to achieve the crack arrest condition in the remainder of the investigation.

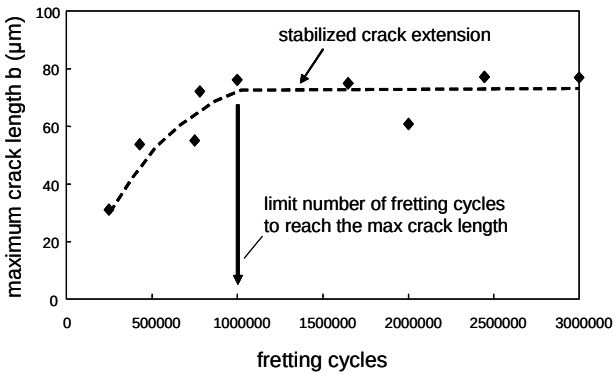

Fig. 5 : Evolution of the crack length versus the fretting cycles (P = 540 N/mm, Q= 283 N/mm). The maximum crack extension below the fretting contact (b = 75 µm) is reached after about 10^6 cycles.*

3.3 Evolution of the crack propagation as a function of the tangential force amplitude.

A second series of fretting tests was performed to identify experimentally the crack length after 10^6 cycles as a function of the applied tangential force amplitude (Q*) and the results are shown in Fig. 6. An approximately parabolic dependence was found, from which the critical tangential force amplitude associated with the crack nucleation (Q_c= 205 N/mm, when b_{exp}=0) could be estimated.

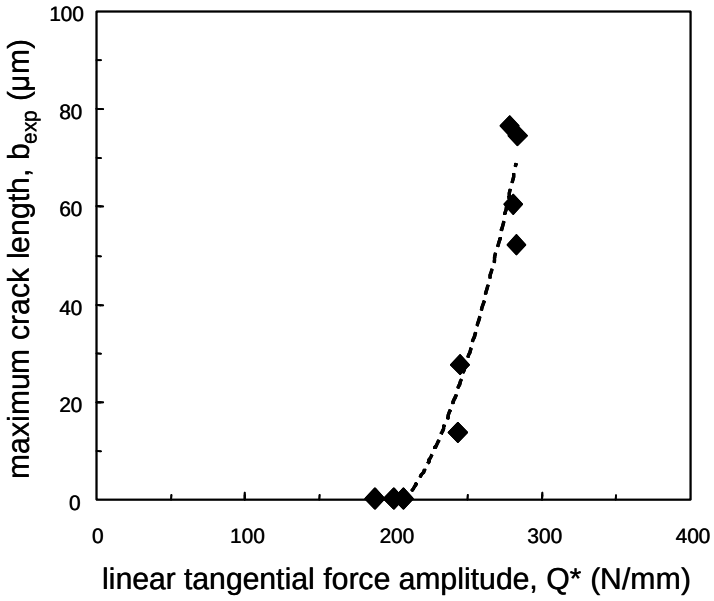

Fig. 5 : Evolution of the maximum crack length identified after 10^6 fretting cycles versus the applied tangential force amplitude (P = 540 N/mm, 10^6 cycles).

3.4 Morphology of the cracks

Before undertaking the crack propagation modeling, it is desirable to examine the crack morphology and, in particular, the crack location and crack propagation direction (Fig. 3). A systematic study concluded that, under partial slip conditions, the crack initiates at the contact edge and propagates inwards at an angle close to 30°±3 to the surface normal. This relatively narrow angle is not usually observed under fretting fatigue conditions because of the dominating effect of the bulk loading, not present here, but means that a mixed mode crack analysis is certainly required.

4. Modelling

4.1 Subsurface stress field analysis

The conditions chosen for the fretting fatigue test were such that linear elastic fracture mechanics contact analyses were appropriate.. The pad radius, R, normal load P and specimen thickness were defined so that each solid could be considered as an elastic half space, and hence the solution for the pressure distribution was Hertzian [17]. Similarly, the subsequent

application of an alternating tangential force gave rise to a symmetric shear traction distribution that is similar to that described by Cattaeno, Mindlin and Deresciewicz [17, 20]. A central stick zone ($|x| < c$) is bordered by regions of microslip. In the absence of an externally-applied fatigue stress, the offset correction to the stick zone position is not required [5]. Also, the contact half width, a, is small compared with the specimen thickness, T, (a/T ≈ 0.05) so that no thickness correction [5] is needed.

Hence by combining the state of stress due to contact pressure (subscript n) and that due to the applied shear (subscript t), the latter obtained using the sliding solution with a corrective shearing traction in the stick region, (σ^n_{ij} σ^t_{ij}) [21], the total stress field developed below the surface when Q(t) = Q* is given by

$$\sigma_{ij}(x,y) = p_0 \left(\frac{\sigma^n{}_{ij}(\frac{x}{a},\frac{y}{a})}{p_0} \right) + \mu p_0 \left(\frac{\sigma^t{}_{ij}(\frac{x}{a},\frac{y}{a})}{\mu p_0} \right) - \mu p_0 \frac{c}{a} \left(\frac{\sigma^t{}_{ij}(\frac{x}{c},\frac{y}{c})}{\mu p_0} \right) \qquad (1)$$

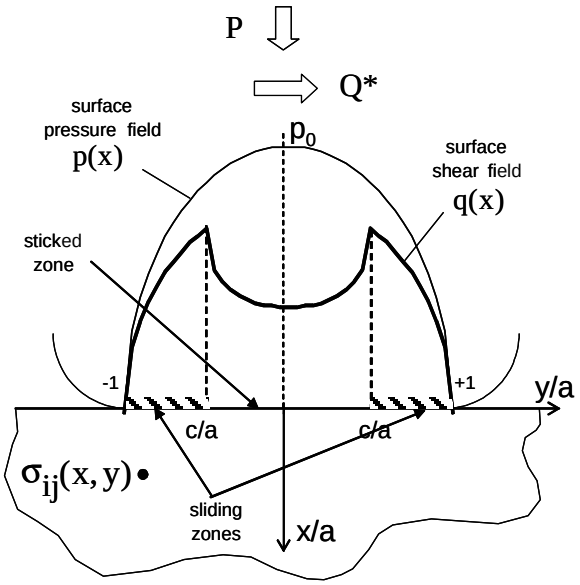

Fig.7 . Illustration of the partial slip cylinder/plane contact loading when Q(t) = Q (c/a =0.5, μ = 0.8)*

4.2 Stress intensity factor

Crack tip stress intensity factors were found using distributed dislocation method which is described in detail in [22]. The technique employs Bueckner's principle [23] which is simply

a superposition principle. Suppose a cracked body is subjected to contact loads as depicted in Figure 8. A problem equivalent to the original would be the superposition of (a) and (b) where (a) represents the body without a crack subjected to the contact load and (b) a cracked body devoid of contact loads but crack line traction and shear equal and opposite to the stress components along the line of the crack so that after summing (a) and (b) the crack faces are traction free. Note that in following this approach we are implicitly making the assumption that the effect of the crack on surface displacements is small, so that the surface tractions remain unchanged by the presence of the crack.

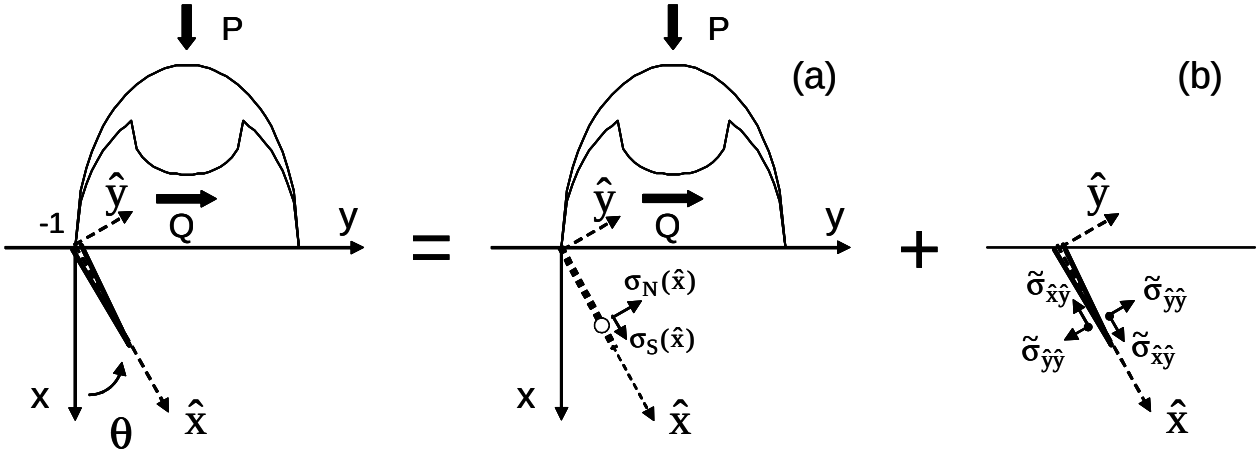

Fig. 8 : Bueckner's principle: (a) Body without crack subjected to contact load, (b) cracked body devoid of external loads but with crack line traction and shear equal and opposite to the crack line stress in (a).

In contrast to an earlier analysis [7, 11], the present investigation clearly requires a slant crack description. Therefore a transformation of stress components is needed in order to determine the unsatisfied tractions (σ_N, σ_T) present along the crack faces. Since, when (a) and (b) are combined, the crack faces have to be traction free we distribute both climb ($b_{\hat{y}}$) and glide ($b_{\hat{x}}$) displacement discontinuities (or "dislocations") along the crack so that the stresses induced ($\tilde{\sigma}_{yy}, \tilde{\sigma}_{xy}$) cancel σ_N and σ_T (Fig. 9).

Published in Engineering Fracture Mechanics, 2008, Vol. 75, p. 1605 - 1622, http://dx.doi.org/10.1016/j.engfracmech.2007.06.011

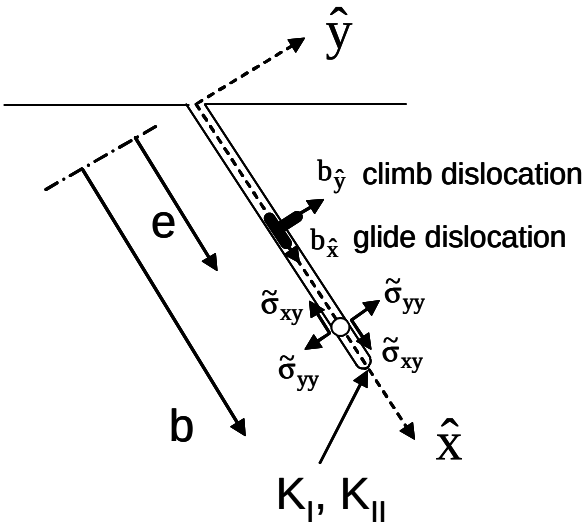

Fig. 9 : Slant crack analysis using climb and glide dislocation distributions to cancel the unsatisfied crack face tractions using Bueckner's superposition principle.

Summing the effect of all the distributed dislocations, we obtain expressions for $\tilde{\sigma}_{\hat{y}\hat{y}}$ and $\tilde{\sigma}_{\hat{x}\hat{y}}$ as function of $b_{\hat{x}}$ and $b_{\hat{y}}$, under plane strain conditions:

$$\tilde{\sigma}_{\hat{y}\hat{y}} = \frac{G}{4\pi(\nu+1)}\left\{b_{\hat{x}}(e)K^{N}_{\hat{x}}(\hat{x},e)+b_{\hat{y}}(e)K^{N}_{\hat{y}}(\hat{x},e)\right\}$$

and

$$\tilde{\sigma}_{\hat{x}\hat{y}} = \frac{G}{4\pi(\nu+1)}\left\{b_{\hat{x}}(e)K^{S}_{\hat{x}}(\hat{x},e)+b_{\hat{y}}(e)K^{S}_{\hat{y}}(\hat{x},e)\right\} \qquad (2)$$

with G and ν the shear modulus and the Poisson coefficients.

The functions $K^{N}_{\hat{x}}$, $K^{N}_{\hat{y}}$, $K^{S}_{\hat{x}}$, $K^{S}_{\hat{y}}$ are the kernels established by the above method. The expressions are lengthy and will not be reproduced here but can be found fully detailed in reference [22, 24]. In contrast to the normal crack, each component of the dislocation induces both shear and direct tractions, so that the solutions for the mode I and II stress intensities are coupled. The integral equations expressing the requirement that the crack faces be traction free are :

$$\sigma_S(\hat{x})+\frac{G}{4\pi(\nu+1)}\left\{\int_0^b B_{\hat{x}}(e)K^{S}_{\hat{x}}(\hat{x},e)\,de+\int_0^b B_{\hat{y}}(e)K^{S}_{\hat{y}}(\hat{x},e)\,de\right\}=0$$

$$\sigma_N(\hat{x}) + \frac{2G}{4\pi(\nu+1)}\left\{\int_0^b B_{\hat{x}}(e)K_{\hat{x}}^N(\hat{x},e)\,de + \int_0^b B_{\hat{y}}(e)K_{\hat{y}}^N(\hat{x},e)\,de\right\} = 0 \qquad (3)$$

where $\sigma_S(\hat{x})$ and $\sigma_N(\hat{x})$ are the resolved shear and normal components of the stress tensor $\sigma(x,y)$ in the $(\hat{x},\hat{y})$ coordinate of the system. It is not possible to solve the equation analytically but powerful numerical quadratures are given in reference [22, 24].

4.3 Definition of an effective stress-intensity range parameter

Because of the compression field imposed by the normal component of contact loading a significant element of crack closure is expected. Therefore a critical issue is the effective stress-intensity range. Most previous fretting fatigue studies consider a pure mode I stress intensity factor associated with a simplified single crack initiated at the contact edge, and which propagates normal to the surface [7, 11]. The present experiment generates a crack at the contact edge but propagating obliquely. Figure 10 shows the normal stress component present along the line of the largest experimental crack detected.

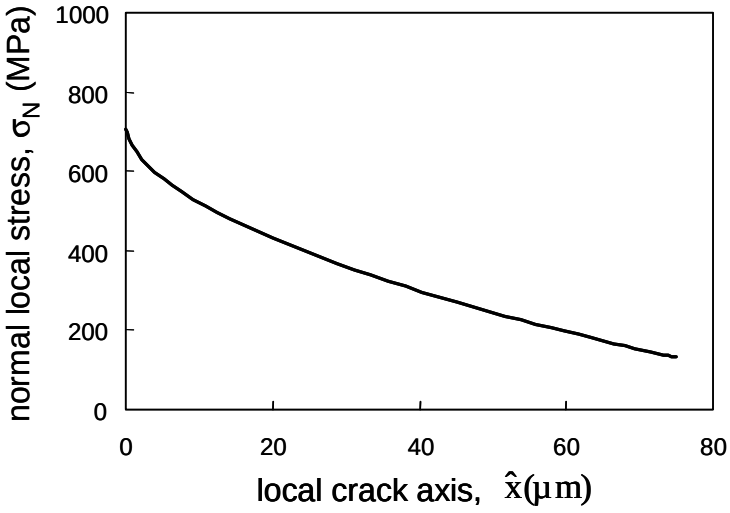

Fig. 10 : Maximum normal stress during the fretting cycle imposed along the crack axis for the maximum crack length experienced (trailing edge, Q= 283 N/mm, θ =30°, b= 75 μm).*

A tensile stress state is present at the trailing edge when the shear force is at a maximum (Q(t) = Q*) which suggests that (for short cracks at least) the crack is open throughout its length.

However, when the shearing force is directed in the opposite sense (Q(t) = -Q*) a pure compressive stress state along the corresponding crack line is generated. This isn't true at the surface, of course. Such a negative stress ratio condition, permit to consider the usual Elber's hypothesis that the effective mode I stress intensity range can be reduced to the maximum stress intensity value (i.e. $\Delta K_{Ieff} = K_{I\,max}$) [16].

In the experiment, the normal load is static, whereas the tangential load varies. Therefore, an effective mode I Stress Intensity Factor (SIF) range may be obtained from the superposition of the contributions from the normal (P) and shear (Q) loads:

$$\Delta K_{Ieff} = K_{I\,max} = K_I^P + K_I^{+Q^*} \qquad (4)$$

Similarly, the alternating tangential force defines a mode II SIF range as :

$$\Delta K_{IIeff} = K_{II}^{+Q} - K_{II}^{-Q} = 2K_{II}^{+Q} \qquad (5)$$

It should be noted that here we are making the implicit assumption that crack face friction is small (i.e. that mode II loading of the crack is unaffected by contact of the crack faces).

Two specific crack angles have been studies: case A, when θ = 0, and case B, when θ = 30:

$$\Delta K_{eff\_A} = \Delta K_{Ieff} \quad (\theta = 0) \qquad (6)$$

$$\Delta K_{eff\_B} = \Delta K_{Ieff} \quad (\theta = 30°) \qquad (7)$$

For the latter case we define a resultant effective stress intensity factor, based on the usual identity for the strain energy release rate:

$$\Delta K_{eff\_C} = \sqrt{\Delta K_{Ieff}^2 + \Delta K_{IIeff}^2} \quad (\theta = 30°) \qquad (8)$$

The different effective stress intensity range formulations versus the normal projection of the crack length are compared in Figure 11.

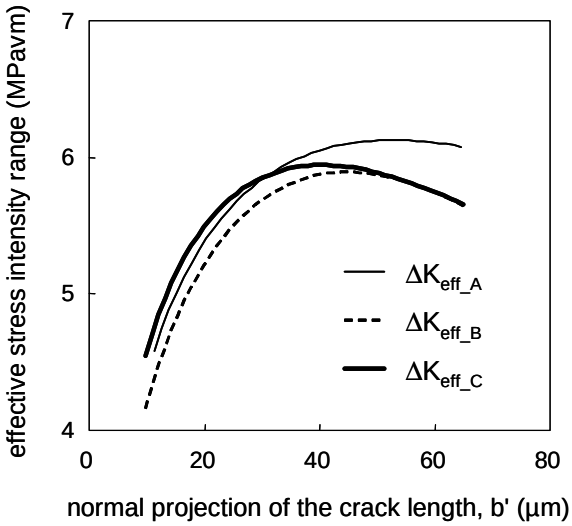

Fig. 11 : Comparison of the effective stress intensity range defined in equations (6) to (8) as a function of the crack length (i.e. reported as the normal projection along x : $b' = b \cdot \cos(\theta)$ *) for the longest experimentally observed crack (trailing edge, 10^6 cycles Q*= 283 N/mm, θ =30°, b= 75 µm).*

Previous investigations show that under uniform stress field ΔK_{eff_A} and ΔK_{eff_B} evolutions are identical [24]. The observed difference between these two quantities in Fig. 11 is only caused by a difference in the stress field crossed by the two crack paths (i.e. $\theta = 0$ and $\theta = 30°$). For a positive angle, the crack is crossing more compressive stress field generated below the contact interface, hence a lower stress intensity factor results. From the resuls shown in Fig 11 it is clear that a simple mode I computation taking into account the crack orientation ΔK_{eff_B} could result in underestimation of the true stress intensity value (i.e. a degree of non-conservatism). In contrast, a pure mode I analysis combined with a normal crack path assumption ($\theta = 0$) tends to overestimate the calculated stress intensity factor, particularly for longer cracks. This may lead to overconservative design. The ΔK_{eff_C} evolution lies between the other two. By using the real crack path it represents the stress experienced by the crack more accurately. Including the mode II contribution using the approach given in equation (8) through its formulation it provides the largest of the three values for short cracks. It should be noted, however, that the difference between the formulations for short cracks is relatively small and may justify the practical application of the normal crack approximation in some circumstances(ΔK_{eff_A}) [9, 11]. However, the

present analysis will nevertheless use the mixed mode formulation (ΔK_{eff_C}) using the following notation:

$$\Delta K_{eff} = \Delta K_{eff\_C} = \sqrt{\Delta K_{Ieff}^2 + \Delta K_{IIeff}^2} \quad (\theta = 30°) \qquad (9)$$

4.3 Short crack methodology

Examination of Fig. 11 suggests that crack propagation may take place in the short crack regime when the effective stress intensity factor ranges is less than the long crack threshold, ΔK_0. We therefore intend to apply the short crack approach, introduced by Araujo et al for fretting fatigue conditions [9]. The starting point is the Kitagawa and Takahashi diagram [13] which shows that many materials exhibit a long crack threshold which is independent of crack length. However, the K-T diagram also shows that cracks can propagate at $\Delta K < \Delta K_0$ provided that the stress is high enough. In a uniform stress field, such short crack behaviour may be interpreted as requiring that the applied stress range is greater than the establish fatigue limit σ_{fl}. As a first approximation the transition crack length (b_0) between short and long crack regimes can be extrapolated by equating these two conditions:

$$\Delta K_0 = 1.12 \cdot \sigma_{fl} \cdot \sqrt{\pi \cdot b_0} \qquad (10)$$

hence,

$$b_0 = \frac{1}{\pi} \cdot \left(\frac{\Delta K_0}{1.12 \cdot \sigma_{fl}} \right)^2 \qquad (11)$$

For the alloy used here, this gives b_0 = 170 µm (since ΔK_0 = 7 MPa√m). Following the approach adopted by Araújo et al., we choose to examine the propagation of the crack in the *modified* K-T diagram (i.e. where ΔK rather than stress is plotted against *b*). This is clearly easier to use in the case where the stress is non-uniform. Hence, the threshold stress, $\Delta K_{th,SC}$ is given by

$$\Delta K_{th,SC} = \Delta K_0 \cdot \sqrt{\frac{b}{b_0}} \qquad b < b_0$$

$$\Delta K_{th,SC} = \Delta K_0 \qquad b > b_0 \qquad (12)$$

Based on this description, the two quantities ΔK_0, and σ_{fl} may be regarded as being the fundamental material properties needed to describe the crack growth under both long and

short crack regimes (Fig. 12). The transition crack length, b_0, may be derived directly from these quantities using equation (11).

5. Results and discussion

An example application of the short crack arrest analysis described above is illustrated in Figure 12. The calculated evolution of stress intensity factor range for the most severely loaded contacts studied (P= 540 N/mm, Q*=283 N/mm) is compared with the short crack threshold obtained from equation (12).

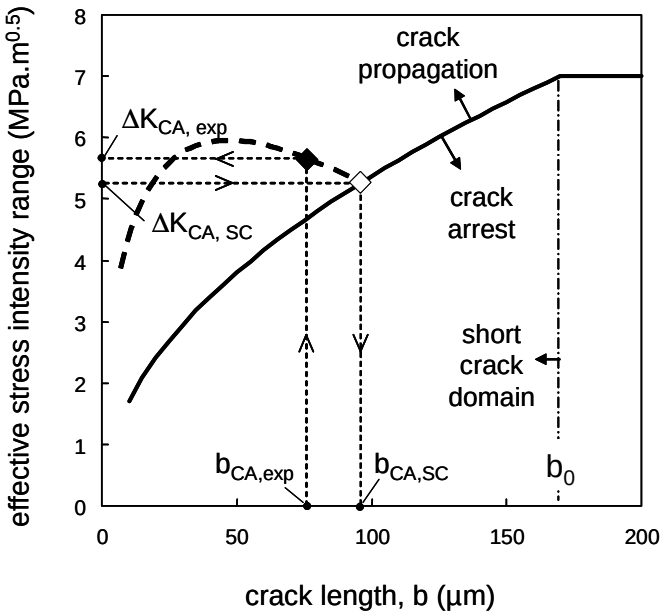

Fig. 12 : Illustration of the fretting crack arrest analysis : —— *crack arrest boundary defined from the short crack formulation* $\Delta K_{th,SC}$ *(Eq. 12);* – – *Evolution of the calculated effective stress intensity range* ΔK_{eff} *as the function of the crack length b (P= 540 N/mm, Q* = 283 N/mm);* ◆ *: Experimental crack arrest condition (*$b_{CA,exp}$*: maximum crack length observed after* 10^6 *fretting cycles);* ◇ *: Crack arrest condition predicted by the short crack arrest approach (*$b_{CA,SC}$*: crack length defined from the intersection between the fretting crack propagation path and the short crack arrest boundary).*

It will be seen from Fig. 12 that for this case the experimentally observed arrested crack length ($b_{CA,exp}$) is reasonably close to that predicted by the short crack arrest approach

($b_{CA,SC}$). To evaluate the more general applicability of the short crack arrest methodology the previous analysis has been generalized to all the experiments studied and the results are presented in Table 2. It will be apparent that the experimental values and the predictions follow the same general trend, but that the short crack approach appears to over-predict the experimentally observed crack lengths, in some cases by a significant amount.

Table 2 : Crack arrest parameters corresponding to the fretting conditions studied (P =540 MPa, μ = 0.9); $b_{CA,exp}$, $\Delta K_{CA,exp}$, $b_{CA,SC}$, $\Delta K_{CA,SC}$: defined in Fig. 12; $\sigma_{VM,CI}$: Maximum Von Mises stress (i.e. before crack initiation) at the crack initiation point induced by the contact loading; $\sigma_{VM,CT}$: Maximum contact Von Mises stress at the point corresponding to the arrested crack tip .

Q* (N/mm)	$\sigma_{VM,CI}/\sigma_{VM,CT}$ (MPa)	$b_{CA,exp}$ (μm)	$\Delta K_{CA,exp}$ (MPa$\sqrt{m}$)	$b_{CA,SC}$ (μm)	$\Delta K_{CA,SC}$ (MPa$\sqrt{m}$)	$\frac{b_{CA,SC}-b_{CA,exp}}{b_{CA,exp}}$ (%)
206	729 / 564	0	-	-	-	-
242	790 / 442	14	4.28	54	3.94	284
243	847 / 285	28	4.98	72	4.62	157
278	850 / 285	77	5.49	93	5.18	21
280	850 / 338	61	5.80	94	5.26	54
282	853 / 376	52	5.92	95	5.28	81
283	854 / 298	75	5.68	96	5.30	28

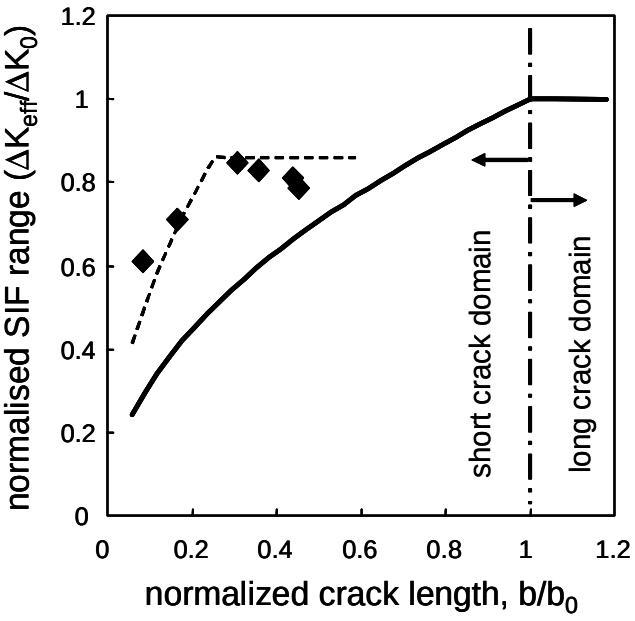

Fig. 13 : Normalised stress intensity factor (SIF) range plotted against crack length: —— theoretical maximum crack extension defined from short crack approach using nominal material parameters(ΔK_0 = 7 MPa$\sqrt{m}$, b_0=170μm)(Eq. 12); – – – theoretical maximum

crack extension obtained using modified parameters (ΔK_0 =6MPa√m, b_{0f}=43μm) (Eq. 12) ◆

Fretting crack experiments modelled using the distributed dislocation method.

Figure 13 displays the experimental crack lengths versus the computed stress intensity factor range. Here, a rather more encouraging picture emerges: it may be seen that the experimental arrested crack lengths follow the same general pattern as predicted by the short crack arrest approach, but that the values for ΔK_0 and b_0 appear to be lower than those used for the short crack analysis. It may be seen that the experimental fretting SIF ranges converge to a 6 MP√m value which is very close to the reference ΔK_0 = 7 MP√m threshold. Given the difficulty in obtaining a reliable value for ΔK_0 from conventional experiments (see, e.g. [25]) this does not seem an excessively large discrepancy. Indeed, the value 6 MP√m is (just) within the range of uncertainty given in [16] (see Table 1). A much larger difference is apparent in b_0, where it appears that a value of around 45μm is required to explain the experimental result, compared to 170μm obtained from nominal material properties (ΔK_0 , σ_{fl}) and equation (11). At first sight it would appear that such a large discrepancy is difficult to explain without resorting to an argument that 'special factors' must apply in a fretting situation. However, it is appropriate to consider the form of equation (11), where it will be seen that b_0 is obtained from ΔK_0, σ_{fl}, and the conventional geometry factor for stress intensity factor by combining these and squaring the result. Each of these quantities is subject to some uncertainty and the power of two exaggerates this effect. Thus, if the modified value of 6 MP√m is accepted for ΔK_0, the predicted value for b_0 would fall from 170 μm to 125 μm. Nevertheless, to obtain a value for b_0 of 45 μm would require a fatigue limit in the region of 450 MPa, which seems unlikely when compared to the experimentally measured value of 270 ± 10 MPa ([16], Table 1). It may be, of course, that despite the initial investigation shown in Fig. 5, the chosen value of 10^6 cycles was not sufficiently large to represent an arrested crack, particularly when one considers the very low crack propagation rates likely in the near-threshold regime.

It is perhaps tempting to define a special fretting fatigue long crack threshold, b_{0f}, but the physical grounds for doing so are rather limited and the experimental evidence presented here is somewhat limited. Hence, we restrict the discussion below to the conventional short crack value of b_0. This is, of course, more conservative and hence potentially very useful for safe

design in the presence of fretting fatigue. We should recognise, of course, that the approach we have followed is purely elastic whereas in practice, some plasticity may be present. To assess the potential importance of plasticity, Von Mises stresses induced by the contact loading at the crack initiation point ($\sigma_{VM,CI}$) and crack tip ($\sigma_{VM,CT}$) points have been computed and reported in Table 2. When compared to the yield stress of the material (Table 1) it appears that the crack nucleation point will experience a considerable degree of plasticity, although, due to the severe drop of the contact stress field below the surface, the crack tip point is located in a nominally elastic region. Hence, a purely elastic model such as that used here would overestimate the stress intensity factor, particularly for small cracks and would account for the calculated ΔK values for the experimental cracks lying above the threshold curve in Fig. 13.

A further consideration concerns the crack modelling procedure itself. The applied methodology is in fact an uncoupled description of the cracking process: The contact stress field is first computed assuming Hertzian / Mindlin contact stress fields and the crack analysis is then carried out using Bueckner's principle. Therefore, it does not capture the alternations to the pressure and shear tractions induced by the presence of a crack. A coupled elasto-plastic model, perhaps obtained using FEM would provide a more complete physical description of the situation. However, such an analysis would require complex and time-consuming computations are difficult to justify, particularly if a simple conservative design approach is required.

Finally, by applying the short crack description described above an inverse numerical procedure has been developed to predict the maximum crack length as a function of the applied tangential force amplitude (Fig. 14).

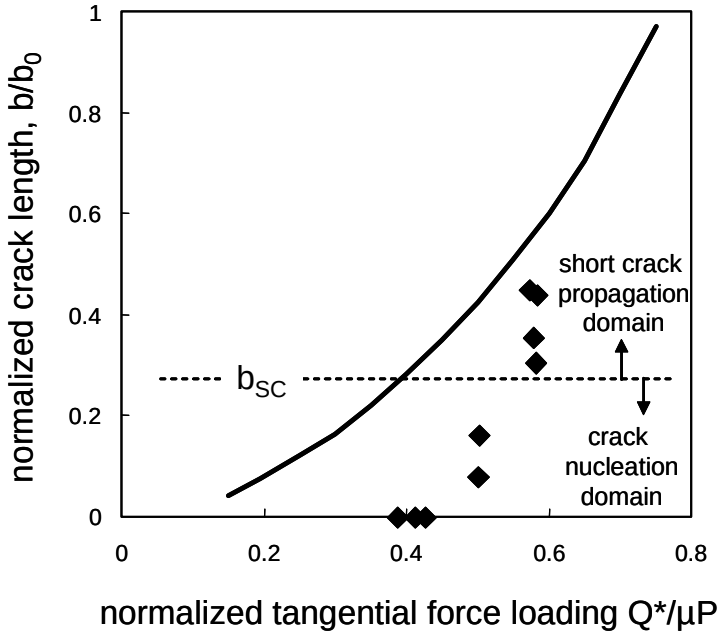

Fig. 14 : Normalized representation of the maximum crack propagation as a function of the imposed tangential force amplitude for the fretting contact studied (AISI 1034/52100 (cylinder), P = 540 N/mm, p_0= 700 MPa, a=500μm, μ=0.9) ; ◆ : fretting experiments; ——— : Theoretical boundary derived from an inverse approach combining the modelling of the slant fretting crack and the short crack arrest approach.

As expected the prediction is conservative (i.e. the observed crack lengths are systematically smaller than the computed ones). It also suggests that a unique crack propagation description is not pertinent for the very short crack domain. Combining the current approach with a crack nucleation method, applied to the shoter crack domain could provide an interesting approach to fully describe the fretting cracking process. In this method, a second crack length variable, defining the transition from initiation to short crack propagation (b_{SC}) is required. Thus there will be a three stage crack history described by the nucleation regime (i.e. $b < b_{SC}$), the short crack propagation regime (i.e. $b_{SC} < b < b_0$), and long crack behaviour (i.e. $b_0 < b$). Future developments may need to focus on this more complex model. However, the approach described in the current paper provides a simplified initial description of fretting crack arrest and permits a quantitative investigation of previous experimental work on this topic (e.g. [26]). It is also expected to favour the coupling analysis between this plain fretting test

condition and the usual fretting fatigue configuration which combines heteregeous fretting and homogeneous fatigue stress fields [27-30].

6. Conclusions

A combined experimental and modelling investigation has been undertaken to investigate the maximum extent of crack propagation under plain cylinder/plane partial slip fretting conditions. The following conclusions may be drawn:

- The material studied displays crack nucleation at the contact edge with a propagation angle of approximately 30° in the partial slip regime.
- Crack growth appears to arrest after approximately 10^6 fretting cycles,
- An analytical model has been implemented, based on a combination of Mindlin's partial slip formalism and a slant crack description using displacement discontinuities. This has shown that a mixed-mode formalism provides a more realistic description of the fretting cracking process. However the relatively small difference observed between this model and the simpler normal crack description, suggests that this latter formulation, may still provide a useful tool for assessment of fretting fatigue cracks.
- The short crack arrest method, initially applied for fretting fatigue endurance predictions by Araujo et al., has been extended to predict the maximum fretting crack extension. The model appears to provide a systematic overestimation of the arrested crack length. However, the magnitude of the discrepancy decreases with increasing arrested crack length. Some of the difference may be attributed to uncertainties in the measured material constants and it is also likely that a degree of plasticity is present in the experiments which is not captured in the model. It is concluded that the short crack methodology is a potentially useful approach for providing conservative predictions of fretting cracking.
- The stabilization of longest fretting cracks for SIF ranges similar to the conventional long crack arrest threshold, ΔK_0, suggests a correlation between fretting cracking processes and classical fatigue description. It also supports the Araujo et al. conjonction that a specific fretting long crack transition should be considered to provide more precise prediction of the crack arrest condition.
- Based on the conservative predictions provided by the short crack arrest methodology, a specific formulation has been implemented to predict the arrested fretting crack length as a function of the applied contact conditions. Reasonable agreement is found with between

experimental and predicted results. It was nevertheless concluded that an approach based solely on crack propagation not sufficient and it is therefore suggested that crack nucleation must be included in order to fully describe the cracking process. Hence, a second crack length variable (b_{SC}) has been introduced to formalize the transition from crack nucleation to short crack propagation.

Finally, it could be outlined the potential interest of a combined analysis between complex but practical fretting fatigue test configurations and more precise but systematical crack arrest plain fretting test situations. However such a perspective is directly related to the development of more complete modeling of the fretting cracking processes involving better considerations of contact plasticity and coupled crack/contact interactions.

References

[1] Hoeppner DW, Chandrasekaran V, Elliot CB, editors. Fretting fatigue: current technology and practices; ASTM STP 1367, American Society for Testing and Materials, 2000, ISBN 0-8031-2851-7.

[2] Waterhouse, R.B., Fretting Fatigue, Applied Science publishers, 1981.

[3] Vincent L, Berthier Y, Godet M. Testing methods in fretting fatigue: a critical appraisal. ASTM STP 1159:33-48, 1992.

[4] Fouvry S, Liskiewicz T, Kapsa Ph, Hannel S, Sauger E. An energy description of wear mechanisms and its applications to oscillating sliding contacts. Wear 2003; 255: 287-298.

[5] Hills DA, Nowell D. Mechanics of fretting fatigue, Dordrecht: Kluwer Academic Publishers, 1994.

[6] Lamacq V , Dubourg M C, Vincent L. A theoretical model for the prediction of initial growth angles and sites of fretting fatigue cracks, Tribology International 1997; 30 (6): 391-400 .

[7] Araújo JA, Nowell D. Analysis of pad size effects in fretting fatigue using short crack arrest methodology, International Journal of Fatigue 1999; 21: 947-956.

[8] Fouvry S, Kapsa Ph, Sidoroff F, Vincent L. Identification of the characteristic length scale for fatigue cracking in fretting contacts, J. Phys. IV France 1998; 8: 159-166.

[9] Araújo JA, Nowell D. The effect of rapidly varying contact stress fields on fretting fatigue. International Journal of Fatigue 2002; 24 (7): 763-775.

[10] Mugadu A, Hills DA, Barber JR, Sackfield A. The application of asymptotic solutions to characterising the process zone in almost complete frictional, International Journal of Solids and Structures 2004; 41 (2):385-397.

[11] Vallellano C., Domínguez J., Navarro A. Predicting the fretting fatigue limit for spherical contact. Engineering Failure Analysis 2004; 11(5): 727-736.

[12] Miller KJ. The two thresholds of fatigue behaviour. Fatigue Fract Eng Mats Structs 1993; 16(9): 931-9.

[13] Kitagawa H, Takahashi S. Application of fracture mechanics to very small cracks or the cracks in the early stage. Philadelphia: American Society for Metals, 1976: 627-630.

[14] El Haddad MH, Smith KN, Topper TH. Fatigue crack propagation of short cracks. Journal of Engineering Materials and Technology 1979; 101: 42-46.

[15] Fouvry S, Duo P, Perruchaut Ph. A quantitative approach of Ti-6Al-4V fretting damage: Friction, Wear and crack nucleation. Wear 2004; 257 (9-10): 916-929.

[16] Gros V. Etude de l'amorçage et de la propagation des fissures de fatigue dans les essieux-axes ferroviaires, D. Phil. Thesis, Ecole Centrale de Paris, France, 1996.

[17] Johnson KL. Contact Mechanics, 1985 (Cambridge University Press, Cambridge).

[18] Fouvry S, Kapsa Ph, Vincent L. Developments of fretting sliding criteria to quantify the local friction coefficient evolution under partial slip condition. 24 th Leeds-Lyon Symposium, Eds. D. Dowson et al , Tribology serie1997; 34: 161-172.

[19] Proudhon H, Fouvry S, Buffière JY. A Fretting crack initiation prediction taking into account the surface roughness and the crack nucleation process volume. International Journal of Fatigue 2005; 27 (5): 569-579.

[20] Mindlin RD, Deresciewicz H. Elastic sphere in contact under varying oblique forces. J Appl Mech 1953, 75:327-344.

[21] Sackfield A, Hills DA. A note on the Hertz contact problem: a correlation of standard formulae. J Strain Analysis 1983; 18 (3): 195-197.

[22] Nowell D, Hills DA. Open cracks at or near free edges. J Strain Analysis 1987; 22 (3): 177-185.

[23] Bueckner HF. The propagation of cracks and the energy of elastic deformation. Trans ASME 1958; 80:1225-1230.

[24] Hills D.A., Kelly, P.A. Dai, D.N, Korsunsky A.M., Solution of crack problems: the distributed dislocation technique, Dordrecht: Kluwer Academic Publishers, 1996.

[25] Moshier, M.A., Nicholas, T.; Hillberry, B.M., 'Load history effects on fatigue crack growth threshold for Ti-6Al-4V and Ti-17 titanium alloys', International Journal of Fatigue, v 23, n SUPPL. 1, 2001, p S253-S258.

[27] Reybet Degat P , Zhou ZR, Vincent L. Fretting cracking behaviour on pre-stressed aluminium alloy specimens. Tribology International 1997; 30 (3): 215-223.

[27] Hutson, AL, Nicholas T. Fretting Fatigue behavior of Ti-6Al-4V against Ti-6Al-4V under flat on flat contact with blending radii. ASTM STP 1367, American Society for Testing and Materials, 2000, ISBN 0-8031-2851-7.

[28] Szolwinski M., Farris T., Mechanics of fretting fatigue crack formation, Wear 1996; 198: 93–107.

[29] Mutoh Y., Xu J.Q., Fracture mechanics approach to fretting fatigue and problems to be solved, Tribology International 2003; 36:99-107.

[30] Namjoshi S.A., Mall S., Fretting behavior of Ti-6Al-4V under combined high cycle and low cycle fatigue loading, International Journal of Fatigue 2001;23: 455-461.